

GINSENOSE CK INHIBITS THE GROWTH OF NON-SMALL CELL LUNG CANCER AND INDUCES APOPTOSIS THROUGH THE EGFR/MTOR PATHWAY *IN VITRO* AND *IN VIVO*Paison Faida^{a,b,d,*}, Linlin Qu^{a,b,c}, Jing Zhao^{a,b}, Xiaoxuan Ma^{a,b}, Rong Huang^c and Daidi Fan^{a,b,*}^aShaanxi Key Laboratory of Degradable Biomedical Materials and Shaanxi R&D Center of Biomaterials and Fermentation Engineering, School of Chemical Engineering, Northwest University, Taibai North Road 229, Xi'an, Shaanxi 710069, China.^bBiotech. and Biomed. Research Institute, Northwest University, Taibai North Road 229, Xi'an, Shaanxi 710069, China.^cShaanxi Giant Biotechnology Co, Ltd, Xi'an, Shaanxi 710076, China.^dSchool of Education, Kigali Independent University, ULK, P.O. Box 2280 Kigali, Rwanda.

*Corresponding Author: Daidi Fan

Biotech. And Biomed. Research Institute, Northwest University, Taibai North Road 229, Xi'an, Shaanxi 710069, China.

Article Received on 15/05/2024

Article Revised on 05/06/2024

Article Accepted on 26/06/2024

ABSTRACT

Lung cancer has become one of the leading causes of cancer-related deaths worldwide, with the most common being non-small cell lung cancer (NSCLC). The current treatment for lung cancer is mainly chemotherapy, but chemotherapeutic drugs generally suffer from severe side effects. Therefore, it is important to find anti-NSCLC drugs that are safe, effective, and with few side effects. Ginsenoside compound K (CK) has not been intensively researched for its potential as a non-toxic therapeutic medication candidate for different kinds of tumors. The effects and functional mechanisms of CK on NSCLC are unknown. We studied the effect and involved mechanism of CK against NSCLC *in vitro* and *in vivo* in this work. First, the MTT experiment, colony formation assay, and cell cycle analysis all demonstrated that CK efficiently suppressed cell proliferation and induced cell cycle arrest. Moreover, Annexin V/PI staining, JC-10 staining, ROS overproduction, western blot, immunofluorescence staining, and TUNEL staining all showed that CK induced apoptosis. Furthermore, this study has shown that CK inhibited the phosphorylation of EGFR, which regulates cancer cell proliferation and apoptosis by mediating downstream PI3K/AKT/mTOR pathway. In addition, ginsenoside CK treatment dramatically suppressed tumor growth in the xenograft nude mice model and caused no injuries. Our study established the anticancer efficacy and mechanism of CK on NSCLC *in vitro* and *in vivo* for the first time, giving basic data supporting CK as a viable therapy for NSCLC.

KEYWORDS: Anti-lung cancer effect, Apoptosis, EGFR signaling pathway, Ginsenoside CK, G1 phase arrest, Xenograft model.

1. INTRODUCTION

Lung cancer is a form of malignant tumor with a high morbidity and death rate that threatens human life.^[1] The most prevalent form of lung cancer, accounting for 80–85% of cases, is non-small cell lung cancer (NSCLC). Adenocarcinoma, squamous cell carcinoma (SCC), and large-cell carcinoma are the three types of NSCLC.^[2] The greatest prevalent histological kind of lung cancer, lung adenocarcinoma has a poor prognosis, low rates of early diagnosis, surgical resection, and postoperative survival rates.^[3] Surgery, chemotherapy, and radiotherapy have been the most widely used methods of therapy in clinical research. However, chemotherapy therapies include several serious adverse effects, including thrombosis, emesis, nausea, alopecia, and

immunosuppression.^[4] To elude the limitations of available treatments for patients with NSCLC currently, There is an urgent need to effectively treat this terrible disease, hence it is essential to create novel medications for lung cancer treatment with few adverse effects. Due to their great efficacy and low risk in lung cancer treatment, drugs produced from natural sources have drawn a lot of attention.^[5] The primary active constituent of ginseng, ginsenoside, has demonstrated excellent pharmacological action, including anticancer properties.^[6] Previous research has shown that the ginsenosides Rg3 and Rk3 reduce proliferation and colony formation, cause cell cycle arrest in the G1 phase, and induce apoptosis by blocking the PI3K/Akt/mTOR pathway in NSCLC and human osteosarcoma.^[7,8]

Ginsenoside Rg5 has shown anti-breast cancer via targeting PI3K.^[9] The primary functional component of ginseng is believed to be the major intestine bacterial metabolite of ginsenosides, known as ginsenoside compound K (CK, 20-O-(D-glucopyranosyl)-20(S)-protopanaxadiol), and has been shown to have a variety of pharmacological effects being a popular research area. Ginsenoside CK has shown the potential to inhibit cell proliferation in breast and liver cancers.^[10,11] However, there was no report about the anticancer properties of ginsenoside CK on H460 and PC9 NSCLC cells.

NSCLC presents with frequent deregulation of the Epidermal Growth Factor Receptor (EGFR) signalling.^[12] EGFR is a receptor located on the surface of cells that enables extracellular signals to enter the cell. Through tyrosine signaling, it modifies the activity of the nucleus. The EGFR is a membrane-bound receptor tyrosine kinase that consists of a ligand-binding extracellular domain, a short hydrophobic transmembrane domain, and a cytosolic domain that possesses tyrosine kinase activity. When proteins bind to the receptor, unique downstream signaling cascades are triggered, which lead to particular functions associated with cell survival, growth, and proliferation.^[13] Studies have revealed a connection between increased expression of the EGFR and various forms of cancer in humans, including NSCLC.^[14] Several studies have found that the expression of EGFR in NSCLC is associated with several negative outcomes, including poor response to chemotherapy, decreased survival, and frequent lymph node metastases.^[15,16] Lung tumor formation may be sparked by EGFR, which promotes pro-survival and anti-apoptotic cellular responses like increased proliferation, angiogenesis, vascular mimicry, and invasiveness.^[17] The translocation of EGFR proteins to the mitochondria is strongly linked to the development of cell death resistance. This phenomenon occurs through the interaction between EGFR and the pro-apoptotic protein PUMA, primarily found within the mitochondria.^[18] However, the effect of ginsenosides, most especially ginsenoside CK, on EGFR expression in NSCLC was not studied. This study presents novel findings regarding the anti-NSCLC effects of ginsenoside CK *in vitro* and *in vivo*. Additionally, the study investigates, for the first time, the molecular mechanism through which CK triggers G1 phase arrest and apoptosis in NSCLC by suppressing the EGFR signaling pathway.

2. MATERIAL AND METHODS

2.1 Materials and chemicals

Ginsenoside CK (Lot#: BP0651) was obtained from Chengdu Biopurify Phytochemicals Ltd. (Sichuan, China), Gefitinib (Cat. No: HY-50895) was obtained from MedChemExpress USA. HyClone (LA, USA) provided the RPMI-1640 (Lot#: SH30809.01) culture medium. GIBCO (NY, USA) supplied the fetal bovine serum (FBS). Xi'an Heart Biological Technology (Xi'an, China) sold the Giemsa staining solution. The Solarbio Science & Technology Co., Ltd. (Beijing, China) offered

the Hoechst 33342 fluorescent dye (Cat No : CA1120). Primary antibodies against Bax (Cat No. 50599-2-Ig), Bcl-2 (Cat No. 68103-1-Ig), c-caspase-3 (Cat No. 68773-1-Ig), c-caspase-9 (Cat No. 10380-1-AP), c-PARP (Cat No. 13371-1-AP), AKT (Cat No. 60203-2-Ig), p-AKT (Cat No. 66444-1-Ig), mTOR (Cat No. 66888-1-Ig), p-mTOR, (Cat No. 67778-1-Ig) PTEN (Cat No. 22034-1-AP), PI3K (Cat No. 67121-1-Ig), p-PI3K (Cat No. 60225-1-Ig), and beta-actin (Cat No. 66009-1-Ig) were purchased from Proteintech (Chicago, IL, USA). AMPK (Cat.No. 2532S), p-AMPK (Cat.#2535T), MEK1/2 (Cat.No. 9122S), ERK1/2 (Cat No. 9102S), P70S6K, RPS6, p-MEK1/2 (Cat No. 9154S), p-ERK1/2 (Cat No. 9101S), p-P70S6K (Cat No. 9205), p-RPS6 (Cat No. 5364S), and Abbkine supplied the secondary antibody IgG. Cell Signaling Technology (Danvers, MA, USA) provided the EGFR (Cat No. 4267S) and p-EGFR (Cat No.3777S). Longyuan Chemical (Zhengzhou, China) supplied the polyethylene glycol (PEG-400), while Aladdin Biotechnology (Shanghai, China) supplied the dimethyl sulfoxide (DMSO) and methyl thiazolyl diphenyl tetrazolium bromide, MTT (Lot#: ST316), MSO (Lot#: ST038) and RIPA lysis buffer (Lot#: P0013B) were purchased from Beyotime Biotechnology (Shanghai, China).. Trypsin (Lot#: T8150), penicillin/streptomycin (Lot#: P1400), crystal violet (Lot#: G1063), PMSF (Lot#: P0100), phosphatase inhibitor cocktail (Lot#: P1260) and BCA protein assay reagent kits (Lot#: PC0020) were purchased from Solarbio Science & Technology Co., Ltd. (Beijing, China). FBS (Lot#: 04-001-1ACS) was purchased from Biological Industries (Kibbutz Beit Haemek, Israel). KeyGen Biotech (Nanjing, China) provided a cell cycle analysis kit, AG-1478 (Cat No. [HY-13524](#)), EGF (Cat No. [HY-P7092](#)), and LY294002 (Cat No. [HY-10108](#)) were purchased from Med Chem Express.

2.1 Cell culture

The non-small cell lung cancer cells (H460 and PC9) were obtained from the American Type Culture Collection (ATCC) situated in Manassas, VA, USA. These cell lines were grown in RPMI-1640 culture medium, supplemented with 10% fetal bovine serum (FBS) and 1% penicillin/streptomycin. Incubation of the cells was carried out at 37 °C under a 5% CO₂ environment.

2.2 Cell viability assay

Cell viability was evaluated using the MTT assay. The H460 and PC9 cell lines were cultured in 96-well microplates at a density of 1×10^4 cells per well and allowed to incubate for 24 hours. Subsequently, the cells were exposed to varying concentrations of CK (0, 40, 50, 60, 70, and 80 μ M) for both 24 and 48 hours. Meanwhile, the control cells were subjected to RPMI-1640 medium supplemented with 10% FBS and 1% penicillin/streptomycin. Following the removal of the supernatant, a solution of PBS containing MTT (5 mg/mL) was added to the cells and allowed to incubate for 3 hours. Afterward, DMSO (150 μ L) was introduced

to each well to dissolve the formazan crystals. Ultimately, the absorbance at 490 nm was gauged using a microplate reader.

2.3 The LDH release assay

The quantification of lactate dehydrogenase (LDH) release was conducted using the lactate dehydrogenase assay kit (Jiancheng Bioengineering, Nanjing, China) by following the provided guidelines. The absorbance was subsequently gauged at a wavelength of 440 nm.

2.4 Colony formation assay

PC9 and H460 cells were introduced into a 6-well plate with a seeding density of 300 cells per well. These cells were subsequently subjected to varying concentrations of CK (0, 40, 50, and 60 μM). The cells were allowed to incubate in a humidified incubator at 37 °C with a 5% CO_2 atmosphere. For every 3-day interval, the culture medium was renewed until observable colonies emerged. Following 14 days, the cells were fixed using 4% paraformaldehyde for 15 minutes, followed by rinsing with PBS and staining with Giemsa for an additional 15 minutes. The quantity of colonies was assessed utilizing ImageJ software.

2.5 Cell cycle analysis

Propidium iodide (PI) staining was employed to investigate the impact of CK on the various phases of the cell cycle. Initially, H460 and PC9 cells were cultured in a petri dish and underwent four passages. Afterward, these cells were propagated in six-well plates at a concentration of 2×10^5 cells/mL for 24 h before exposure to CK (0, 40, 50, and 60 μM). Subsequently, adherent and suspended cells were collected using Trypsin-EDTA (Sigma-Aldrich) and then fixed overnight at 4 °C in 75% ice-cold ethanol. Once fixed, the cells were subjected to staining with 50 $\mu\text{g/mL}$ PI and 100 $\mu\text{g/mL}$ RNase A in the dark at 37 °C for 30 minutes. Flow cytometry (Becton Dickinson, CA) was employed to measure the fluorescence intensity of individual cell nuclei, and the acquired data were analyzed using FlowJo software.

2.6 Annexin V/PI staining assay

PC9 and H460 cells were placed into a six-well plate with a density of 2×10^5 cells per well. These cells were subjected to treatment with CK at varying concentrations (0, 40, 50, and 60 μM) for a duration of 24 h. Subsequent to this incubation period, the cells were harvested and suspended in a binding buffer. A staining solution composed of Annexin V and PI was utilized to label the NSCLC cells, which were then allowed to incubate in darkness at 37 °C for 15 minutes. Ultimately, flow cytometry was employed for the examination of the stained cells.

2.7 Hoechst 33342 staining assay

Apoptosis was investigated through the utilization of Hoechst 33342 staining. H460 and PC9 cells were grown into a six-well plate with a density of 2×10^5 cells per

well. Following this, the cells were exposed to CK at various concentrations (0, 40, 50, and 60 μM) for a span of 24 h. After the treatment period, the cells underwent two washes with chilled PBS and were then subjected to incubation with Hoechst 33342 (10 $\mu\text{g/mL}$, Solarbio, Beijing, China) for a duration of 15 to 20 minutes. The cellular morphology was subsequently examined utilizing an inverted fluorescence microscope (Nikon, Japan) equipped with UV illumination.

2.8 Mitochondrial membrane potential assay

To assess the influence of CK on mitochondrial membrane potential (MMP), the JC-10 Assay Kit (Beyotime, Jiangsu, China) was employed. H460 and PC9 cells were grown into a six-well plate with a seeding density of 5×10^5 cells per well. These cells were subjected to treatment with CK at varying concentrations (0, 40, 50, and 60 μM) for a duration of 24 h. Subsequent to the treatment period, the cells were collected and exposed to JC-10 at a temperature of 37 °C for 20 minutes. The flow cytometry technique was then utilized to gauge the decline in MMP. The ratio of red to green fluorescence intensity served as an indicator for the assessment of mitochondrial depolarization.

2.9 AO/EB staining assay

NSCLC cells were grown uniformly at a density of 5×10^5 cells per well in six-well plates and exposed to CK (0, 40, 50, and 60 μM) for 24 h. Subsequently, a dual acridine orange/ethidium bromide (AO/EB) mixture from Solarbio, China, was used to stain the cells. The stained cells were then incubated in a six-well plate at room temperature and kept away from light for 10 min. Lastly, the cells were observed under a fluorescence microscope.

2.10 Detection of intracellular ROS

To detect intracellular reactive oxygen species (ROS) production, 2',7'-dichlorodihydrofluorescein-diacetate (DCFH-DA) staining was performed. PC9 and H460 cells were seeded at a density of 5×10^5 cells per well in six-well plates and exposed to CK (0, 40, 50, 60 μM) for 24 h. The cells were then washed with serum-free medium and stained with 10 μM DCFH-DA at 37 °C for 25 min. The production of ROS was detected with an inverted fluorescence microscope (Nikon, Japan).

2.11 Western blotting

H460 and PC9 cells were grown into a six-well plate with a density of 5×10^5 cells per well and allowed to incubate overnight. Following this incubation period, the cells were exposed to CK at varying concentrations (0, 40, 50, and 60 μM) for a duration of 24 h. Both cell samples and tumor tissues underwent lysis on ice for a span of 35 min, utilizing RIPA (Radio-Immuno Precipitation Assay) buffer (Beyotime, Shanghai, China) supplemented with 1% PMSF, 1% phosphorylation inhibitors (Solarbio, China), and 1 mM phenylmethylsulfonyl fluoride (PMSF). After lysis, the cell lysates were centrifuged for 20 minutes at 4 °C,

utilizing a speed of 12,000 rpm. Protein quantities within the supernatant were measured using the BCA Assay kit from Thermo Fisher, Shanghai, China. SDS-PAGE was employed to segregate the proteins, with the subsequent polyvinylidene fluoride (PVDF) membranes utilized for this purpose. After being blocked using 5% nonfat milk in TBST for 2 hours at room temperature, the membranes were subjected to overnight incubation at 4 °C with the appropriate primary antibodies. On the subsequent day, the membranes were washed five times with 1 TBST and then incubated with HRP-conjugated secondary antibodies for a period of one hour at room temperature. Protein bands were visualized using the Tanon ECL system (Shanghai, China). The protein bands were quantified by ImageJ software, by drawing a box around the protein band and quantify the signal within the box. Volume boxes were drawn around the bands of interest in such a way that they include all of the intensity of the band with a minimal amount of surrounding background.

2.12 NSCLC xenograft nude mouse model

To investigate the therapeutic benefits of ginsenoside CK on non-small cell lung cancer *in vivo*, a tumor-bearing nude mouse model was designed. All experimental protocols followed the People's Republic of China's Animal Ethics protocols and Guidelines and were authorized by Northwest University's Animal Ethics Committee. Hunan SJA Lab Animal Co., Ltd. provided female nude mice aged 5 weeks. These mice were chosen with care and housed in a sterile environment. A one-week phase shift of the light/dark cycle was applied to the animals, and they were provided unrestricted access to a portion of standard food. The H460 xenograft model was built by injecting a cell suspension containing 1×10^7 cells in 200 μ L of FBS-free medium into each mouse's left axilla. When visible tumors formed, often within one week, successful tumor implantation was proven. Based on tumor size and body weight, the tumor-bearing mice were randomly divided into four groups: (1) Control group: Mice received a daily intraperitoneal (i.p) injection of 0.9% saline solution. (2) Low-dose CK-treated mice received an intraperitoneal injection of CK at a dose of 30 mg/kg/d. (3) High-dose CK-treated mice received an intraperitoneal injection of CK at a dose of 60 mg/kg/d. (4) Gefitinib-treated mice were given 50 mg/kg/d of gefitinib intragastrically (i.g). The mice were given treatment every day for 27 days, during which time the tumor volumes were calculated using the formula: $[1/2 \times a \times b]$, where "a" represents the tumor's long diameter and "b" represents the tumor's short diameter. To track the progression of the mice in each group, their body weights and tumor volumes were assessed twice a week. After the 27th day of the treatment period, all mice were sacrificed, and their tumor tissues were carefully removed, weighed, and collected for further analysis.

2.13 Hemogram assay and measurement of biochemical parameters

On the 27th day of the study, blood samples were procured from each cohort of mice and transferred into

tubes containing ethylenediaminetetraacetic acid (EDTA). These collected blood samples were then subjected to analysis to evaluate diverse hematological markers, which encompassed the quantification of white blood cells, lymphocytes, and granulocytes. For this analysis, an automated hematology analyzer (HC2200, Meiyilinm, China) was used. Simultaneously on the 27th day, serum samples were also collected from every group of mice. These serum samples were used for the assessment of various indicators of renal function, including urea, uric acid (UA), and creatinine, in addition to parameters of liver function such as alanine transaminase (ALT) and aspartate transaminase (AST). In order to obtain accurate measurements of these parameters, commercial kits sourced from Shanghai Enzyme Biotechnology Co., Ltd (Shanghai, China) were utilized, following the instructions provided by the manufacturer.

2.14 Histopathology and Immunohistochemistry

The organ index was determined using the formula: organ index = organ weight/body weight. Histopathological examination and immunohistochemistry were conducted as follows. Tumor tissues and major organs such as the heart, liver, spleen, lung, and kidney were fixed in 4% paraformaldehyde and subsequently embedded. Thin sections of 5 μ m were prepared and stained with hematoxylin and eosin (H&E) to visualize tissue morphology. Additionally, an immunohistochemistry assay was performed to assess the expression of Ki67 in the tumor tissues. Images of the stained sections were captured using a microscope from Nikon (Tokyo, Japan).

2.15 Immunofluorescence assay (IF)

After adhering to the slides, H460 and PC9 were incubated together with varying concentrations of CK for 24 h. Following fixation, the cells were blocked with 5% bovine serum albumin, and treated with primary and secondary antibodies. The fluorescence intensity analysis and visualization of the sections were performed using an Olympus fluorescence microscope from Nikon (Japan).

2.16 TUNEL assay

To detect apoptosis in tumor tissues, the TUNEL assay was performed as follows. Initially, the tissues were fixed by immersion in a solution containing 4% paraformaldehyde at 4°C for 4–24 h. Following fixation, the tissues were cryosectioned into thin slices measuring 5 μ m. The sections underwent permeabilization with 0.2% Triton X-100 and were exposed to a TUNEL reaction mixture comprising nucleotides and terminal deoxynucleotidyl transferase (TdT) for one hour at 37°C. Afterward, the stained cells were washed with PBS and examined using a Nikon fluorescence microscope.

2.17 Statistical analysis

Statistical analysis was conducted utilizing either the GraphPad Prism 8.0 software package or the SPSS 19.0

software package from SPSS Inc., USA. The data were expressed as the mean \pm standard deviation (SD) derived from three or more distinct samples. Statistical significance was established for p-values less than 0.05 ($P < 0.05$).

3. RESULTS

3.1 Ginsenoside CK suppresses the growth of NSCLC cells

To study the inhibitory effect of ginsenoside CK on NSCLC cells, PC9 and H460 cells were incubated with different concentrations of CK for 24 h and 48 h, and cell viability was detected by MTT assay. Compared with the control, the results revealed that CK remarkably decreased the viability of PC9 and H460 cells in a dose and time-dependent manner (Fig. 1A and B). In addition, the IC₅₀ values in PC9 and H460 cells treated with CK for 24 h were 57.09 μ M and 58.12 μ M, respectively. To further explore the cytotoxicity of ginsenoside CK on H460 and PC9 cells, we examined the release of lactate dehydrogenase after ginsenoside CK treatment of H460

and PC9 cells. The leakage of lactate dehydrogenase (LDH), an indicator of cell membrane damage and cytotoxicity was determined by colorimetric assay. Compared to the control, the percentage of LDH leakage in PC9 and H460 cells was increased in a dose-dependent manner, demonstrating the occurrence of cell membrane damage and cytotoxicity (Fig. 1C). Moreover, a colony formation assay was performed, which showed that CK decreased the colony formation capacity of PC9 and H460 cells in a dose-dependent manner. The findings of the colony formation assay have demonstrated that PC9 and H460 cells treated with CK formed fewer and smaller colonies in a dose-dependent manner compared to the control (Fig. 1D and E). Furthermore, the AO/EB double staining was performed to confirm further the effects of ginsenoside CK on PC9 and H460 cell viability. AO/EB staining assay revealed that the number of cells that displayed red-orange fluorescence was concentration-dependently greater in both treated H460 and PC9 cells (Fig. 1F). These results strongly suggested that CK inhibited PC9 and H460 cell growth.

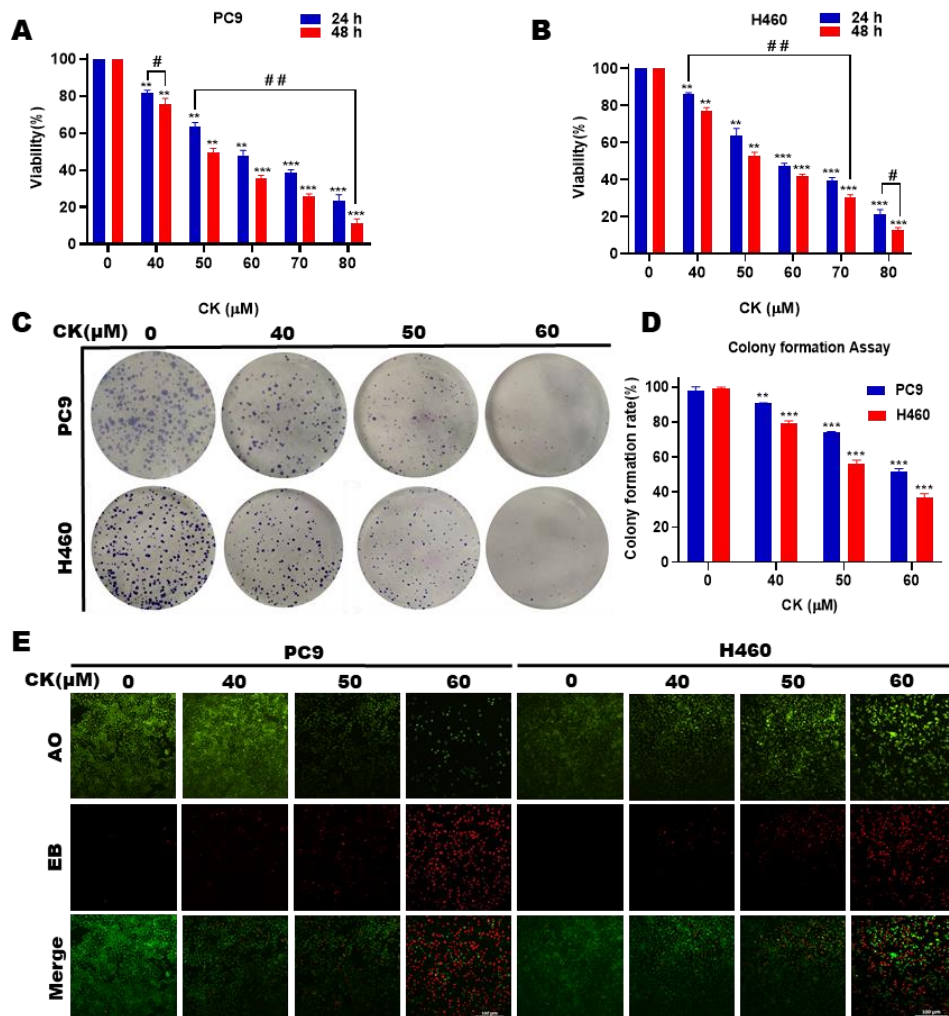


Fig. 1: CK suppressed NSCLC cell viability *in vitro*. The cell viability of (A) PC9 and (B) H460 cells. (C) Lactate dehydrogenase release assay. (D) The colony formation assay of H460 and PC9 cells. (E) Histogram results of colony formation assay. (F) AO/EB staining via fluorescence microscopy. Data are presented as the means \pm SD of triplicate experiments, * $P < 0.05$, ** $P < 0.01$, *** $P < 0.001$ compared with the control; # $P < 0.05$, ## $P < 0.01$, ### $P < 0.001$ compared same concentrations of CK treatment between 24 h and 48 h.

3.2 CK suppresses effectively the growth of H460 xenograft tumors

In this experiment, H460 cells were selected to establish NSCLC tumor xenograft model to explore the *in vivo* inhibition effect of ginsenoside CK on NSCLC. After the successful establishment of the H460-xenograft tumor-bearing model, the intraperitoneal injection was performed to observe the effect of ginsenoside CK on the tumor volume of H460-xenograft tumor-bearing nude mice and the inhibitory effects of CK on tumor progression was studied *in vivo*. During the whole experimental process, all tumor-bearing nude mice did not die. Gefitinib was used as a positive control due to its authorization as the primary treatment option for advanced non-small cell lung cancer patients. After 27 days of treatment initiation, tumor growth was significantly inhibited compared to the control group. Tumor size reduction (shrinkage) was observed in both treated groups as the response of the treatment in a dose-dependent manner (Fig. 2A), and the growth of the H460

xenograft tumors was suppressed in the CK-treated groups and the gefitinib-treated group (Fig. 2C and E). These findings suggest that CK has potential as a therapeutic agent for the treatment of non-small cell lung cancer. Furthermore, the H&E staining results have shown that the tumor cells in the control group were intact and tightly arranged, whereas the tumor cells treated with CK and gefitinib notably declined, with lighter staining, partial degeneration, and necrosis. It can be seen from H&E staining of tumor tissues of tumor-bearing nude mice that ginsenoside CK inhibits tumor growth of NSCLC tumor cells in tumor tissues (Fig. 2F). In addition, the expression of Ki67, a molecular marker associated with cell proliferation, was assessed. The Ki67 expression levels in the high-dose CK-treated and the gefitinib-treated groups were significantly reduced compared to the control group (Fig. 2G). These results indicated that CK suppressed human non-small cell lung cancer growth *in vivo*.

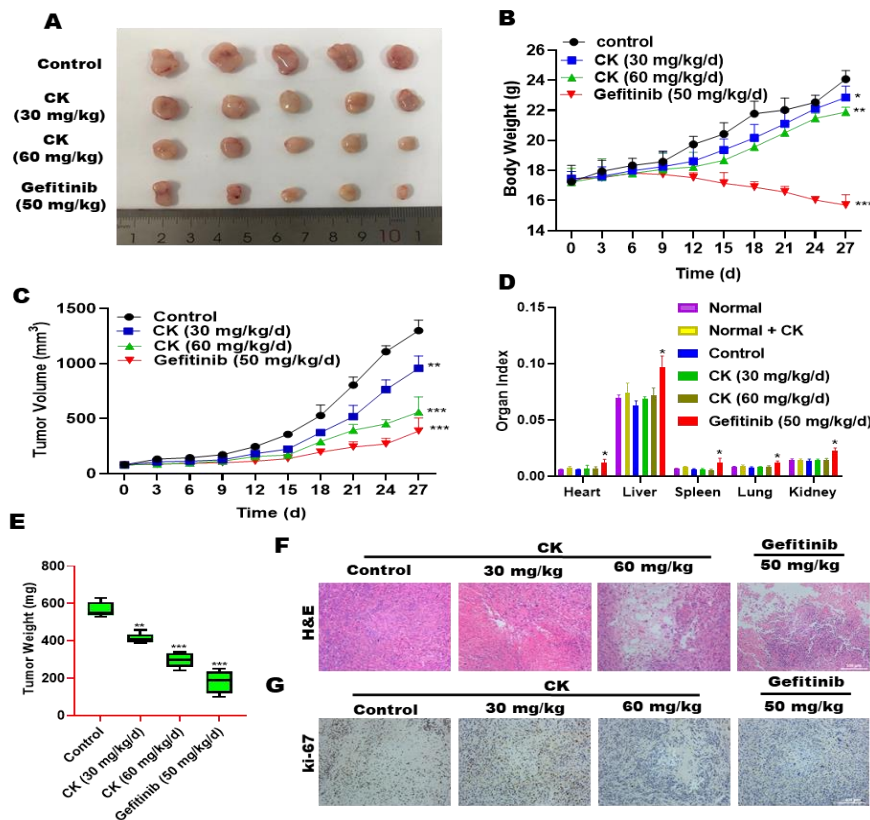


Fig. 2. Ginsenoside CK significantly inhibited the proliferation of tumors in H460 subcutaneous tumor-bearing mice. (A) Representative image of H460-xenograft tumor. (B) Body weight. (C) The tumor volume. (D) The data of organ index. (E) Tumor weight. (F) H&E staining of tumor tissue. (G) Immunohistochemistry assays. All data are presented as the means \pm SD (n=3), *** $P < 0.001$ compared with the control.

3.3 Toxicity evaluation of CK in the xenograft nude mice

The toxicity of CK was assessed in xenograft nude mice by calculating the organ index of vital organs such as the heart, liver, lung, spleen, and kidney. Both the control group and CK-treated groups showed no significant

differences in organ index compared to the normal group, indicating the absence of CK toxicity (Fig. 2D). Moreover, during the initial 6 days of treatment, the administration of CK did not affect the body weight of mice. Both the CK-treated mice and control mice exhibited progressive weight gain. Notably, the body

weight of mice in the CK-treated groups was higher than mice in the gefitinib-treated positive control group, indicating gefitinib toxicity. However, the CK-treated groups did not exhibit any differences compared to the normal group (Fig. 2B). The proportions of immune cells in peripheral blood samples were also evaluated to further determine CK toxicity. There were no significant variations in the number of white blood cells (WBC), lymphocytes (LYM), and granulocytes (GRAN) between the normal, normal + high-dose CK, control (untreated), low-dose CK, and high-dose CK groups. In contrast, the number of immune cells in the gefitinib group was lower than in the control group (Fig. 3A), indicating that gefitinib may disturb the immune system, whereas CK had no adverse effects on the immune system. Additionally, the impact of CK on liver and kidney functions was investigated. After 27 days of CK administration, there were no significant differences in liver function parameters (ALT and AST) or renal

function parameters (urea, uric acid, and creatinine) compared to the control group. Therefore, CK did not have an adverse effect on the liver or kidneys (Fig. 3B and C). In contrast, liver function parameters in mice treated with gefitinib were significantly elevated, indicating the side effects of gefitinib on the liver. Furthermore, H&E staining displayed no apparent unreasonable variations in the normal appearance of main organs (heart, liver, spleen, lung, and kidney) in the normal group, normal + CK (high dose) group, untreated group, and CK-treated groups. On the other hand, the organs in the gefitinib-treated group exhibited various abnormalities, such as vacuolization surrounding hepatocyte nuclei, collapsed alveolar structures, widened alveolar septa, and disorders in the renal structure (Fig. 3D). Our findings suggest that CK does not disrupt the normal functioning of main organs and immune cells in nude mice.

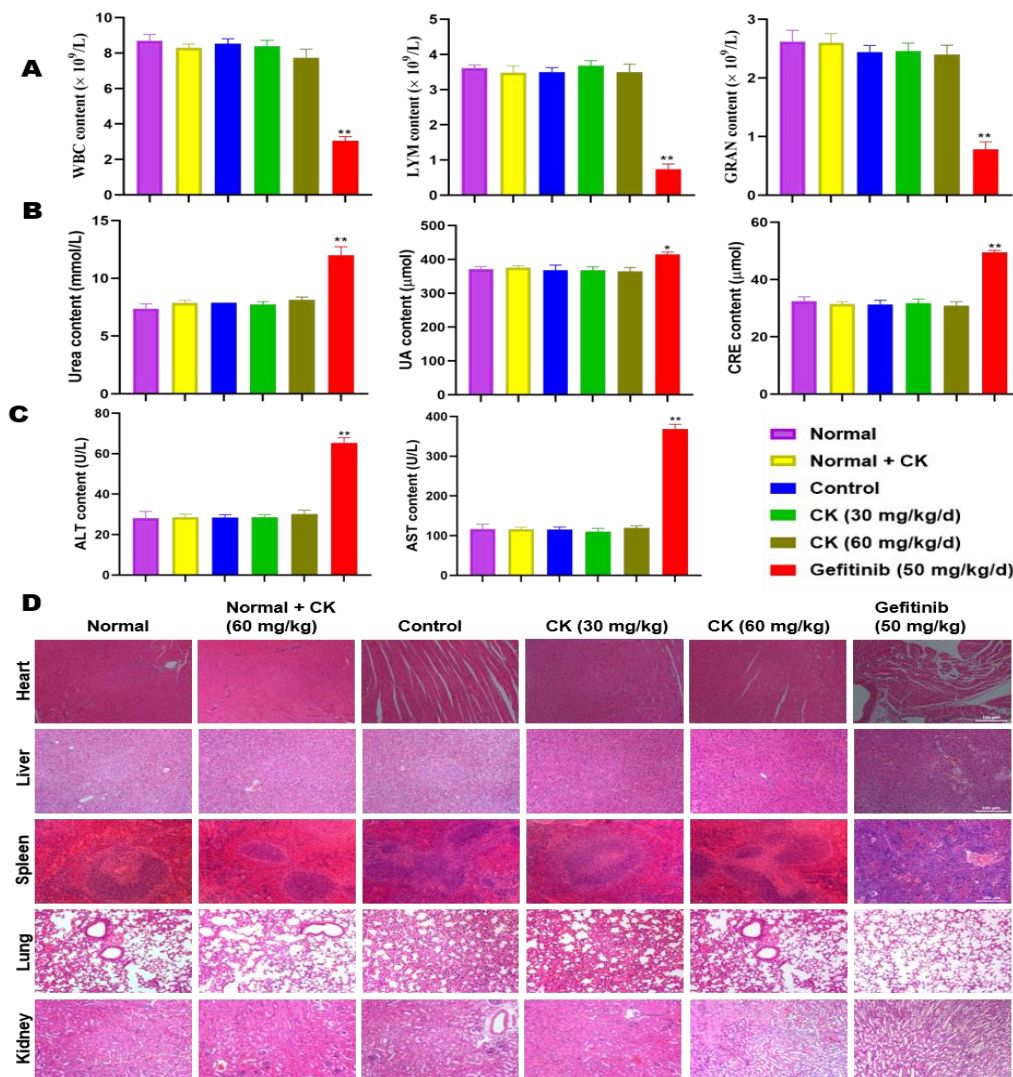


Fig. 3: Effect of CK on vital organs of tumor-bearing nude mice. (A) The number of white blood cells (WBC), lymphocytes (LYM,) and granulocytes (GRAN) in the peripheral blood sample of each group. (B) The levels of renal function parameters (urea, Uric acid, and Creatine) and (C) liver function parameters (ALT and AST) in the serum from each group. (D) H&E staining of the main organs. All data are presented as the means \pm SD (n=3), *** $P < 0.001$ compared with the control, Scale bar = 100 μ m.

3.4 Effect of CK on cell cycle distribution in NSCLC

To demonstrate whether the effect of CK on the proliferation of NSCLC cells was related to cell cycle distribution, flow cytometry, and western blotting were used to verify the effect of CK on the cell cycle in the PC9 and H460 cells. Flow cytometry analysis revealed that, following 24 h of CK treatment, the proportion of cells in the G1 phase increased, while the proportions of cells in the S and G2 phases gradually decreased compared to the control group. Notably, the highest concentration of CK (60 μ M) led to an increase in the number of cells in the G1 phase and a decrease in the number of cells in the S and G2 phases compared to the control group. Specifically, CK treatment increased the proportion of cells in the G1 phase from 73.38% to 93.97% in H460 cells, while decreasing the percentage of cells in the S phase from 9.61% to 5.9% and the percentage of cells in the G2 phase from 5.6% to 5.1%. Similarly, in PC9 cells, the proportion of cells in the G1 phase increased from 56.3% to 86.84%, while the proportion of

cells in the S, and G2 phases decreased from 15.57%, and 14.8% to 4.37%, and 12.06%, respectively (Fig. 4A and B). Flow cytometry findings revealed that CK has the potential to inhibit tumor growth by inducing cell cycle arrest in non-small cell lung cancer cells. To further investigate the ability of CK to induce G1 arrest in NSCLC cells, the expression of proteins associated with the cell cycle arrest at the G1 phase was examined by western blotting assay. CK treatment of H460 and PC9 cells resulted in significant protein increases in p21 and p53, while a significant decrease in CDK4 and cyclin D1 protein expression was observed in a dose-dependent manner (Fig. 4C). Moreover, identical results were obtained in tumor tissues from the low-dose CK-treated group, the high-dose CK-treated group, and the gefitinib-treated group in terms of G1 phase-associated protein expression (Fig. 4D). Our findings suggest that CK inhibits the growth of NSCLC cells and tumor tissues by arresting the cell cycle at the G1 phase in PC9 and H460 cells and tumor tissues.

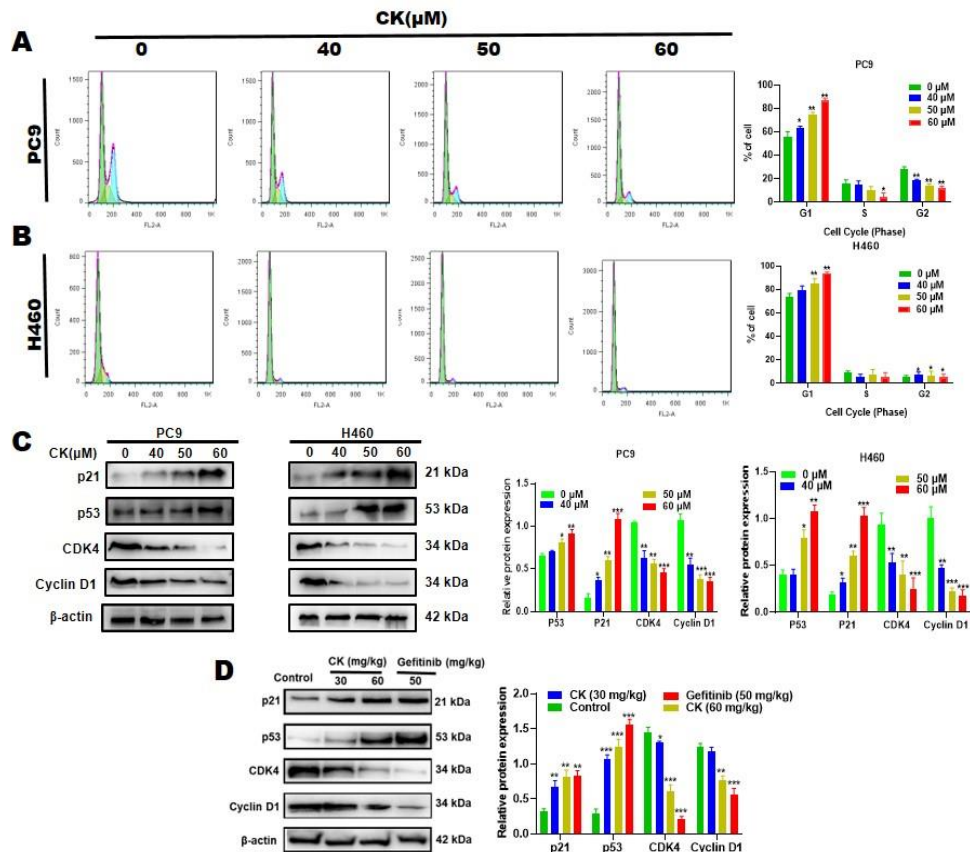


Fig. 4: CK induces G1 phase arrest of NSCLC cells. (A) Flow cytometry analysis of cell cycle distribution in PC9 and (B) H460 cell lines. (C) The expression of the G1 phase arrest-related proteins and (D) tumor tissues. All data are presented as the means \pm SD (n=3), * $P < 0.001$ compared to the control.**

3.5 CK induces caspase-dependent apoptosis in non-small cell lung cancer

To investigate if the suppression of cell proliferation was attributed to apoptosis, non-small cell lung cancer cells were subjected to CK treatment for 24 h and subsequently stained with Annexin V/PI. Flow cytometry analysis was performed to examine the cells. The

findings demonstrated a substantial dose-dependent increase in the percentage of apoptotic H460 and PC9 cells following CK treatment, confirming apoptosis activation (Fig. 5A). Moreover, the main apoptotic protein expressions in NSCLC cells were investigated. Following overnight incubation of NSCLC cells, treatment with different concentrations of ginsenoside

CK for 24 h resulted in increased levels of Bax, cleaved caspase-3, c-caspase-9, and c-PARP, while Bcl-2 levels decreased in a dose-dependent manner in both H460 and PC9 cells. These findings indicate that CK activates apoptosis in NSCLC cells (Fig. 5B and C). Similar results were observed in tumor tissues of non-small cell lung cancer (Fig. 5D). To further validate the apoptotic effect of ginsenoside CK on NSCLC cells, a pan-caspase inhibitor called Z-VAD-FMK, which inhibits caspase activity was used. PC9 and H460 cells were pretreated with Z-VAD-FMK at a concentration of 60 μM for 2 h, followed by treatment with ginsenoside CK at a concentration of 50 μM. The MTT experiments demonstrated that Z-VAD-FMK significantly reversed the cell death induced by ginsenoside CK. Upon pretreatment with the Z-VAD-FMK inhibitor, the cell viability of PC9 and H460 cells treated with ginsenoside CK exhibited significant increases, rising from 63.7%

and 65.7% to 74.3% and 78.2%, respectively. These results showed noteworthy differences compared to the cells treated with ginsenoside CK alone (Fig. 5E). Moreover, the impact of ginsenoside CK on the expression of apoptotic proteins in PC9 and H460 cells following Z-VAD-FMK pretreatment is depicted in Figure 5F. Z-VAD-FMK significantly impeded the expression of cleaved caspase-3 and cleaved PARP proteins in PC9 and H460 cells, as compared to NSCLC cells treated solely with ginsenoside CK. In PC9 and H460 cells co-treated with Z-VAD-FMK and ginsenoside CK, the expressions of cleaved caspase-3 and cleaved PARP proteins were significantly reduced, showing significant differences (Fig. 5F). Taken together, these results suggest that CK induces caspase-dependent apoptosis in non-small cell lung cancer in both *in vitro* and *in vivo*, with the extent of apoptosis being dependent on the concentration of CK.

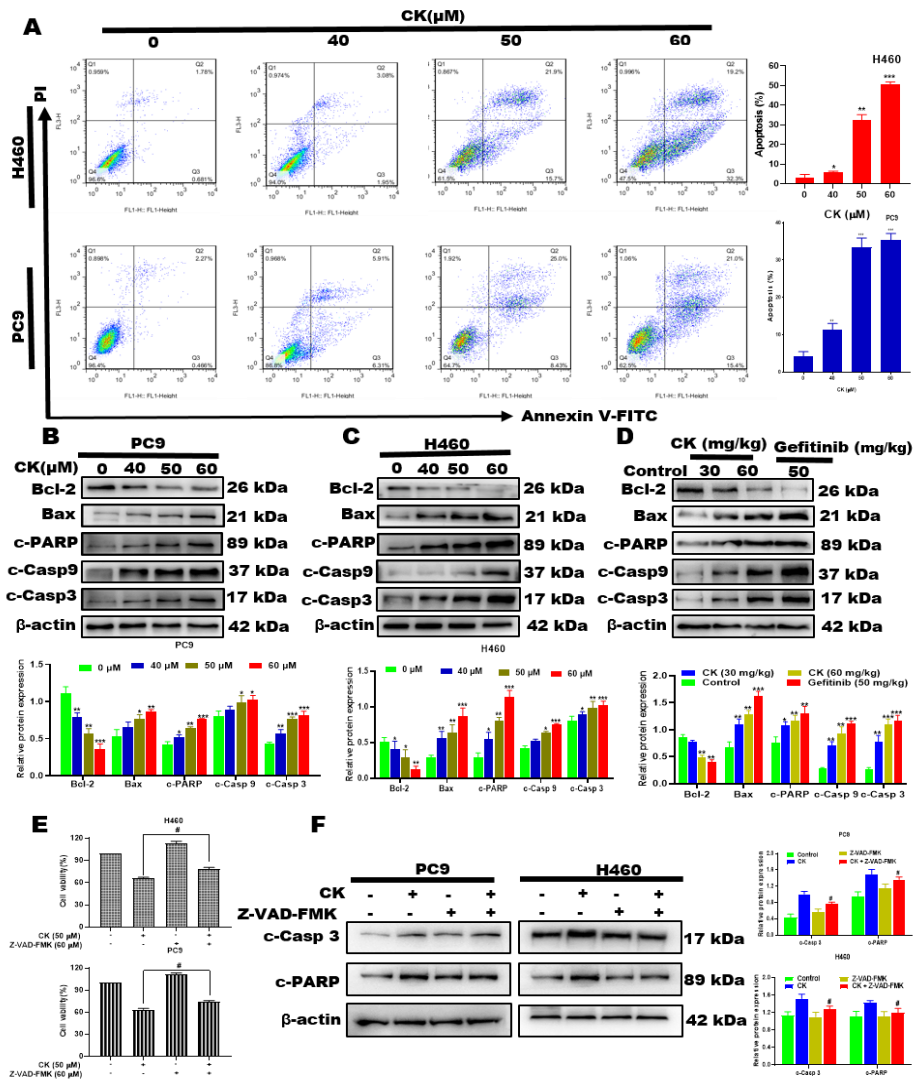


Fig. 5: *In vitro* and *in vivo*, CK caused NSCLC cells to undergo apoptosis. (A) Analysis of flow cytometry. Apoptosis-related proteins were identified by Western blotting in (B) H460, (C) PC9 cells and (D) tumor tissues. (E) NSCLC cells were exposed to CK (50 M) while Z-VAD-FMK (60 M) was present. Cell viability was assessed by the MTT test. (F) Western blot analysis was used to evaluate the expression levels of cleaved PARP and casp-3. * $P < 0.05$ and ** $P < 0.01$ as compared with the control group. # $P < 0.05$ and ## $P < 0.01$ as compared with CK-treated cells. Values are expressed as mean \pm SD (n = 3).

3.6 CK induces ROS generation and apoptosis via a mitochondrial-mediated pathway

We investigated whether CK-induced apoptosis in NSCLC cells was mediated through the mitochondrial apoptotic pathway. The mitochondrial membrane potential was assessed using the fluorescent mitochondrial probe JC-10. Flow cytometry analysis showed a significant decrease in the red/green fluorescence intensity ratio in H460 and PC9 cells after CK treatment compared to the control, showing mitochondrial depolarization (Fig. 6A). We used Hoechst 33342 fluorescence staining to confirm that the decrease of NSCLC cell proliferation was driven by apoptosis. The nuclei of untreated cells showed an intact pale blue staining, indicating that the cell shape and condition were unaffected. However, the number of cells with contracted chromatin and fragmented fluorescent nuclei increased dramatically in a concentration-dependent manner after CK treatment. CK-treated cells exhibited bright fluorescent nuclei, indicating apoptosis and demonstrating that CK reduced cell numbers and increased the formation of apoptotic bodies (Fig. 6B). Furthermore, to evaluate the production of reactive

oxygen species, which plays an essential role in cellular apoptosis, we assessed the impact of CK on ROS production using DCFH-DA staining. Flow cytometry analysis of cells stained with the membrane-impermeable probe DCFH-DA, which is converted into the fluorescent derivative DCF, revealed an elevation in ROS levels. An appropriate level of intracellular ROS promotes cellular proliferation, while excessive ROS production can lead to oxidative stress and cell apoptosis. CK significantly increased the intracellular ROS level in both PC9 and H460 cells in a concentration-dependent manner (Fig. 6C). Additionally, TUNEL staining was performed to confirm CK-induced apoptosis in tumor tissues. The control group exhibited very few apoptotic PC9 cells, whereas the CK-treated groups and the gefitinib-treated group showed a dose-dependent increase in TUNEL-positive H460 cells (Fig. 6D). The experimental results provided compelling evidence that CK stimulates the production of ROS and initiates caspase-dependent apoptosis through the activation of the mitochondrial apoptotic pathway in non-small cell lung cancer in a dose-dependent manner.

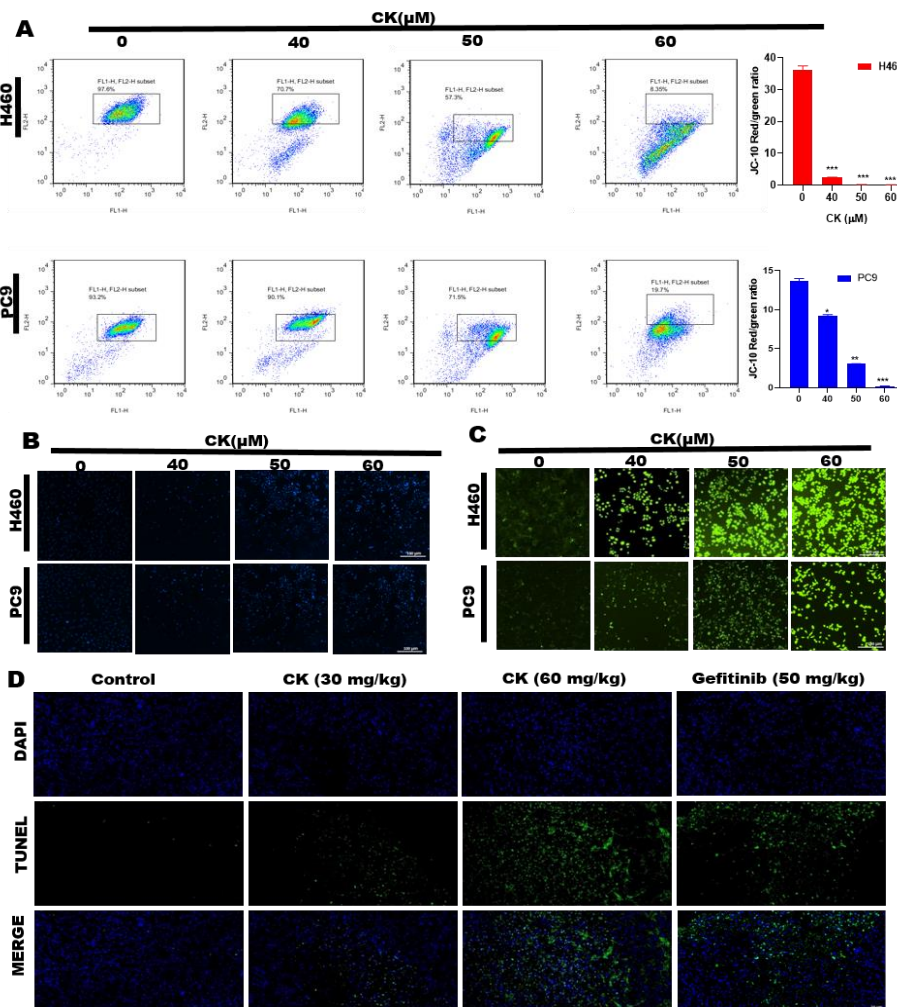


Fig. 6: Ginsenoside CK induced apoptosis of NSCLC cells *in vitro* and *in vivo*. (A) Flow cytometry. (B) H460 and PC9 cells were stained with Hoechst 33342, Scale bar = 100 μm. (C) The intracellular ROS levels, Scale bar = 100 μm. (D) TUNEL staining of tumor tissues, Scale bar = 50 μm.

3.7 EGFR/AMPK signaling pathway involved in CK-induced cell apoptosis *in vitro* and *in vivo*

The epidermal growth factor receptor (EGFR), a transmembrane glycoprotein, is one of the tyrosine kinase receptors in the ErbB family. Dimerization activation causes the phosphorylation of auto-tyrosine kinases, which activates the downstream signaling proteins of EGFR, stimulating cell proliferation, survival, and apoptosis.^[20] The EGFR/MAPK pathway is an important signaling pathway that plays a wide range of functions in biological and pathological processes.^[21] This work investigated whether or not CK induced H460 and PC9 cell apoptosis via the EGFR signaling pathway. Western blotting was performed, and the results have shown that CK significantly inhibited the phosphorylation of EGFR, MEK1/2, ERK1/2, P70S6K, and RPS6, and markedly induced the phosphorylation of

AMPK, which are the downstream kinases of the EGFR pathway (Fig. 7A, C, and D). Moreover, similar results were found in tumor tissues; both EGFR, MEK1/2, ERK1/2, P70S6K, and RPS6 were detected to be relatively constant, and the extents of their phosphorylation were found to have decreased, but markedly p-AMPK was found to have increased (Fig. 7B, and E). Furthermore, we also evaluated the expression of the EGFR and p-EGFR proteins in tumor tissues by immunofluorescence staining (IF). The results exhibited a remarkable difference in the expression of p-EGFR between the control group, the ginsenoside CK-treated groups, and the gefitinib-treated group (Fig. 7F and G), indicating that CK suppressed the expression of p-EGFR. However, the expression EGFR was constant in all groups.

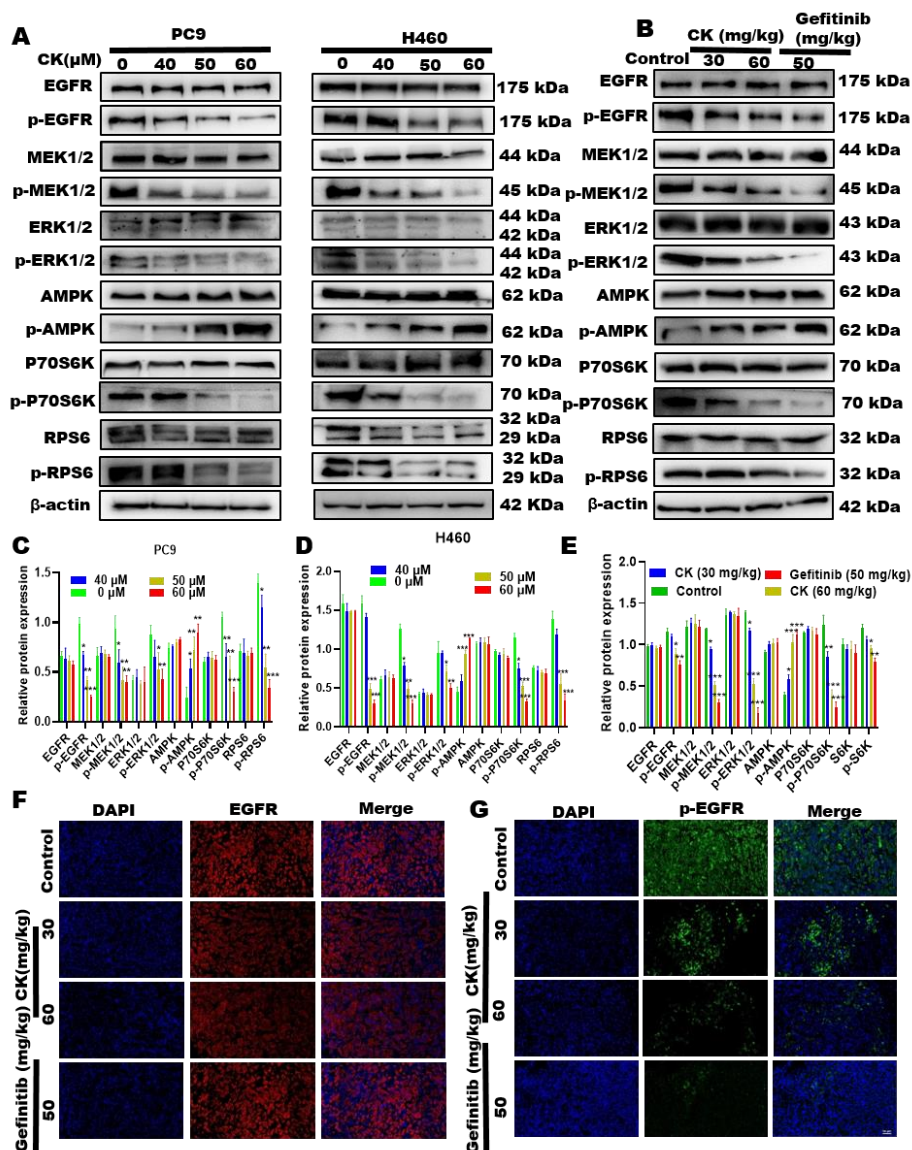


Fig. 7: Effects of CK on the EGFR signaling pathway in PC9 and H460 cells. The protein expression of the EGFR pathway in (A) PC9 and H460 cells and (B) tumor tissues. (C-D) Histogram of protein expression in cells and (E) tumor tissues. (F-G) Immunofluorescence staining for EGFR and p-EGFR in tumor tissues, scale bar = 50 μm. Values are expressed as mean ± SD (n = 3), *P < 0.05, **P < 0.01, ***P < 0.001 compared with the control.

In addition, to confirm the role of EGFR in this process, we evaluated cell viability in combination treatment of CK and AG-1478 (an EGFR inhibitor) or EGF (an EGFR activator). After pretreatment with AG-1478 (200 nM) or EGF (100 ng. mL⁻¹) for 2 h and then followed by cotreatment with CK (50 μM) for another 24 h, the MTT results showed that EGF partially reduced the inhibitory effects of CK on NSCLC cells. In contrast, the AG-1478 enhanced the inhibitory effect of CK on NSCLC cells compared to the effect on NSCLC cells treated only with CK (Fig. 8A and B). The expression levels of EGFR, MEK1/2, ERK1/2, p-EGFR, p-MEK1/2, and p-ERK1/2

protein were then determined by western blotting. EGF pre-treatment has affected the effect induced by CK in NSCLC cells by increasing the expression of p-EGFR, p-MEK1/2, and p-ERK1/2 to stimulate cell growth and inhibit cell apoptosis (Fig. 8C). Nevertheless, pretreatment with AG-1478 significantly enhanced the reduction of the protein expression of p-EGFR, p-MEK1/2, and p-ERK1/2 and had a minor effect on EGFR, MEK1/2, and ERK1/2 compared to the effects of 50 μM CK alone (Fig. 8D). The findings from this study suggest that CK promotes cell apoptosis in NSCLC cells through the EGFR pathway *in vitro* and *in vivo*.

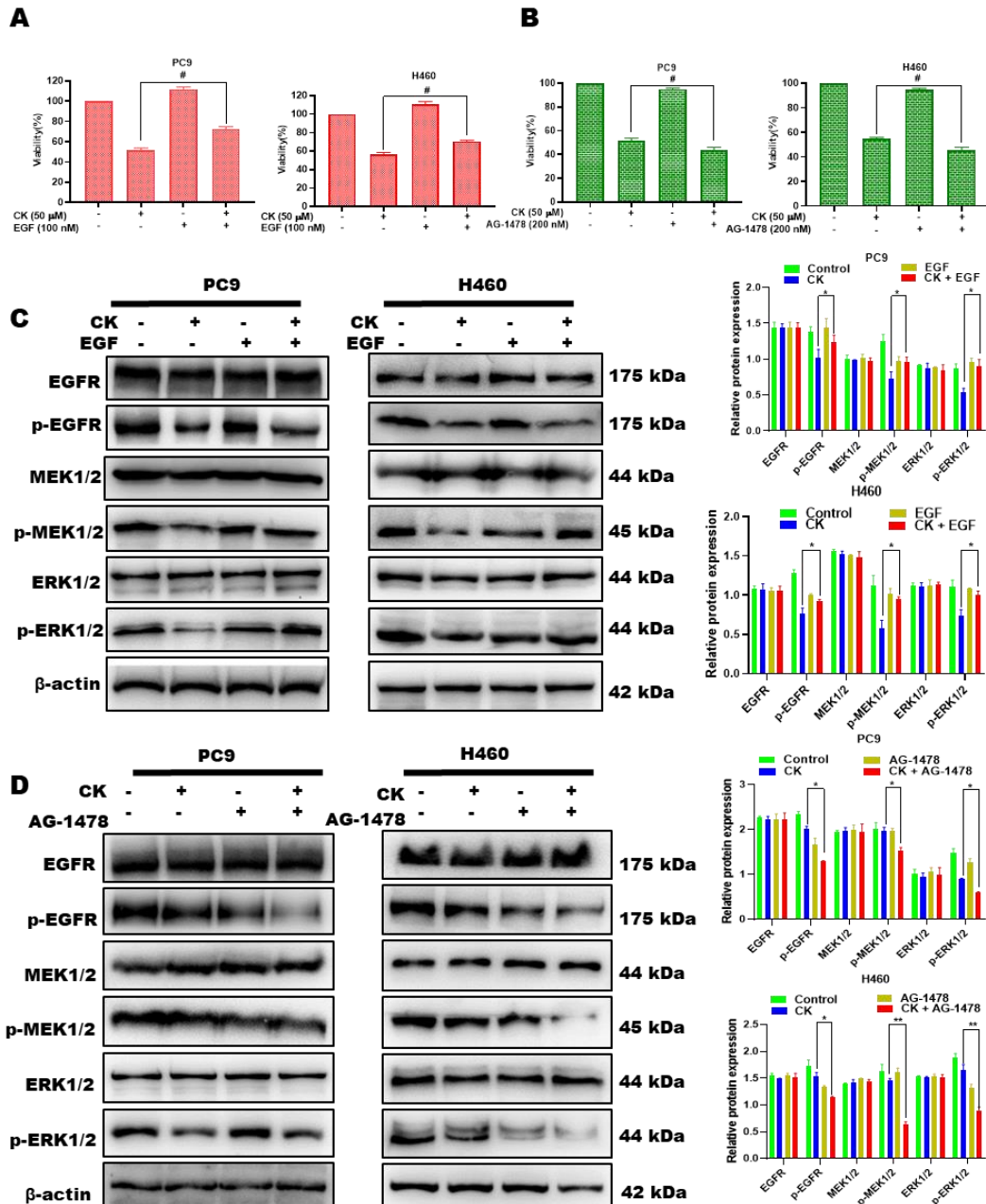


Fig. 8: Effects of ginsenoside CK on the EGFR signaling pathway in NSCLC cells. PC9 and H460 cells were treated with CK (50 μM) with or without AG-14780 (200 nM) or EGF (100 ng mL⁻¹), respectively. (A, B) Cell viability was determined by the MTT assay. (C, D) The protein levels were determined by western blotting. All data are presented as means ± SD from at least three independent experiments. **P* < 0.05, ***P* < 0.01, compared with control, #*P* < 0.05, ##*P* < 0.01, compared with the CK-treated group.

3.8 CK induces apoptosis through the PI3K/Akt signaling pathway

The PI3K/PTEN/Akt/mTOR pathway, which acts as a significant signaling pathway downstream of growth factor receptor tyrosine kinases, has garnered significant interest due to its involvement in numerous essential cellular processes. This pathway is particularly appealing as a therapeutic target, as it governs vital functions such as cell growth, survival, proliferation, motility, apoptosis, and autophagy.^[22] The stimulation of EGFR plays a crucial role in enhancing the survival, metastasis, and proliferation of glioma cells by triggering the PI3K/Akt/mTOR pathway, specifically activating the mammalian target of rapamycin complex 1 (mTORC1) cascade.^[23] Thus, western blotting was performed to investigate whether CK induced apoptosis in H460 and

PC9 cells through the inhibition of the PI3K/PTEN/Akt/mTOR pathway. The study examined the expression levels of PTEN, PI3K, Akt, and mTOR, as well as their phosphorylated forms. The findings indicated that CK treatment did not significantly affect the expression of PI3K, Akt, and mTOR. However, it noticeably increased the expression of PTEN while decreasing the levels of phosphorylated PI3K, Akt, and mTOR (Fig. 9A, C, and D). Similar findings have been identified in tumor tissues (Fig. 9B, and E). Moreover, immunofluorescence staining results showed a remarkable decrease in the expression of p-PI3K in the ginsenoside CK-treated and gefitinib-treated groups compared to the control group (Fig. 9F), indicating that CK suppressed the expression of p-PI3K.

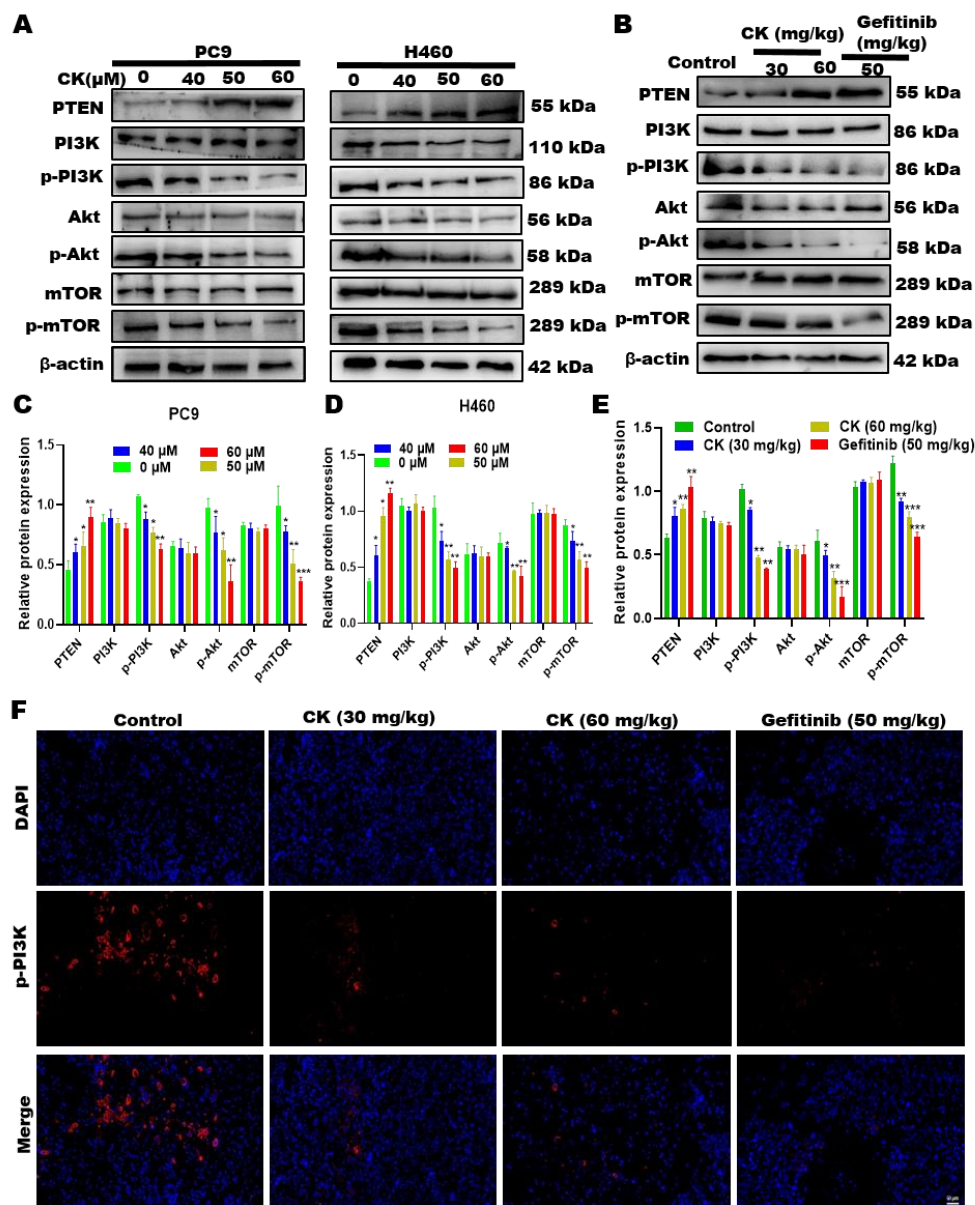


Fig. 9: CK suppressed PI3K/mTOR pathway *in vitro* and *in vivo*. (A-E) The protein expression of PTEN/PI3K/Akt/mTOR pathway in cells and tumor tissues. (F) Immunofluorescence staining for p-PI3K in tumor tissues, scale bar = 50 μm. Values are expressed as mean ± SD (n = 3), *P < 0.05, **P < 0.01, ***P < 0.001 compared with the control.

Furthermore, to investigate the role of the PTEN/PI3K/Akt/mTOR pathway in the regulation of NSCLC cell apoptosis, we used LY294002 (a PI3K inhibitor). Pretreatment with LY294002 (20 μ M) could increase cytotoxicity (Fig. 10A). In addition, western blotting results indicated that the phosphorylation of PI3K, Akt, and mTOR was reduced, while PTEN

expression was increased (Fig. 10B). Our findings revealed that CK induced cell apoptosis in NSCLC cells and tumor tissues by promoting the expression of PTEN and repressing the phosphorylation of PI3K, Akt, and mTOR, which confirms that ginsenoside CK inhibited the PI3K/AKT/mTOR pathway to induce apoptosis in NSCLC.

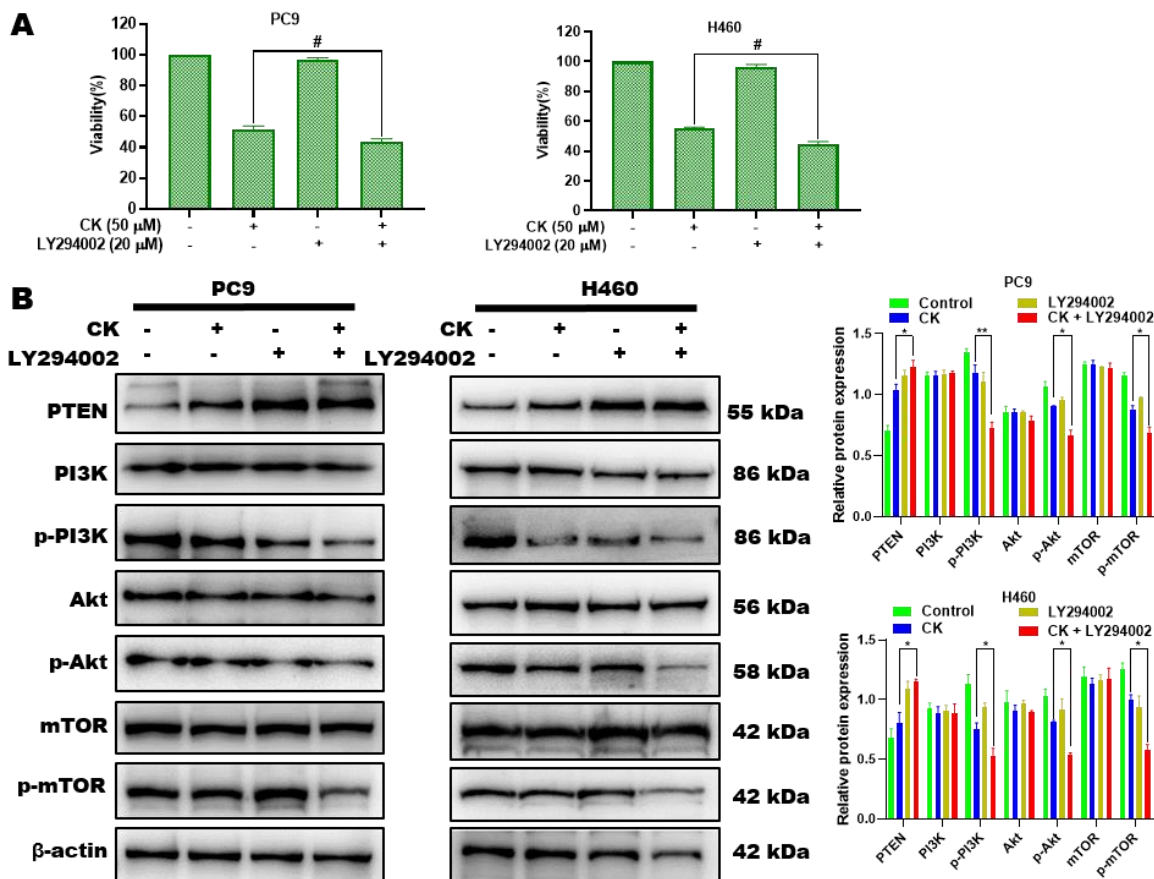


Fig. 10. Effects of ginsenoside CK on the EGFR signaling pathway in NSCLC cells. PC9 and H460 cells were treated with CK (50 μ M) with and without LY294002 (20 μ M), respectively. (A) Cell viability was determined by MTT. (B) The levels of PTEN, PI3K, Akt, mTOR, p-PI3K, p-Akt, and p-mTOR were analyzed. Proteins were determined by western blotting. All data are presented as means \pm SD from at least three independent experiments. * $P < 0.05$, ** $P < 0.01$, compared with control, # $P < 0.05$, ## $P < 0.01$, compared with the CK-treated group.

4. DISCUSSION

Chemotherapy is currently the major strategy of treatment for lung cancer; however, it frequently has negative side effects that make it difficult to treat lung cancer, especially NSCLC. Cisplatin and other platinum-based drugs, including carboplatin, ormaplatin, and oxaliplatin, have demonstrated successful treatment outcomes in numerous human cancers. However, a significant number of patients experience relapse, often attributed to drug toxicity and/or resistance. These adverse effects can impact multiple organs, such as the liver, kidneys, gastrointestinal tract, cardiovascular system, hematologic system, and nervous system.^[24] Gefitinib, classified as an EGFR-TKI (epidermal growth factor receptor tyrosine kinase inhibitor), has been authorized as the primary treatment option for patients

diagnosed with advanced non-small cell lung cancer (NSCLC).^[25] *In vivo* studies have shown that gefitinib is metabolized in the liver and characterized by its tolerability and rapid tumor response, but it has most of the adverse effects, including rash, dry skin, and diarrhea, are mild to moderate in severity and are reversible.^[26,27] As a result, we urgently seek new therapeutic strategies; ginsenoside CK has demonstrated effective anticancer properties in a variety of tumors. Extensive mechanistic studies have shown that CK suppressed cancer cell growth by inducing cell cycle arrest, apoptosis, inhibiting angiogenesis, and sensitizing colon cancer, and neuroblastoma cells and showed no toxicity to the major organs.^[28,29] Nevertheless, the specific effect of CK on NSCLC and the underlying molecular mechanisms have not been investigated.

Therefore, this study aimed to examine the anticancer properties of CK in NSCLC by assessing its effects on cell proliferation, cell cycle progression, and apoptosis in NSCLC cells as well as in a xenotransplantation model of non-small cell lung cancer.

The MTT, colony formation, and AO/EB experimental findings revealed that CK suppressed the proliferation of H460 and PC9 cells *in vitro* after treatment for 24 h. In xenograft tumor-bearing mice of H460 cells, CK significantly inhibited tumor growth. Furthermore, ginsenoside CK demonstrated a notable decrease in the expression of ki-67 within the tumor tissues, suggesting its inhibitory effect on tumor growth. These findings collectively indicate that CK exhibits anti-non-small cell lung cancer activity both *in vitro* and *in vivo*. In addition, in the CK treatment groups, the results obtained from H&E staining revealed that the administration of CK at both low and high doses did not disrupt the normal functioning of the vital organs. Serum biochemical parameter assay results have shown that liver function parameters and renal function parameters in the CK-treated groups have no significant difference compared with the normal group. Moreover, the hemogram study demonstrated that CK did not reduce the amount of immune cells in all groups' peripheral blood samples, indicating the absence of immune damage caused by CK. Furthermore, our animal study findings indicated that mice treated with CK had higher body weights compared to those treated with gefitinib, indicating the absence of toxicity associated with CK. Thus, these results strongly indicate that CK exhibits no adverse effects in the treatment of non-small cell lung cancer. Inducing cell cycle arrest as a means to inhibit cancer cells has proven to be an efficacious approach in lung cancer treatment. The cell cycle is the time elapsed between the ending of one division of a rapidly multiplying cell and the start of the next division. Cancer is characterized by abnormal cell cycle protein activity and uncontrolled tumor proliferation. As a result, cell cycle protein regulation-induced cell cycle arrest is seen as an appealing target for cancer treatment. In this study, the utilization of ginsenoside CK treatment for 24 h resulted in an increased percentage of PC9 and H460 cells in the G1 phase, as observed through flow cytometry analysis. Conversely, there was a decrease in the proportion of cells in the S and G2 phases, indicating G1 phase arrest. The progression of the cell cycle is primarily orchestrated by a well-coordinated interplay involving three key classes of proteins: cyclin-dependent kinases (CDKs), cyclins (Cyclins), and cyclin kinase inhibitors (CKIs). Notably, pivotal roles within the G1/S checkpoint of the cell cycle are fulfilled by proteins p53 and p21. Meanwhile, the seamless advancement of the cell cycle from the G1 to the S phase hinges on the regulatory functions of CDK4 and cyclin D1.^[30] Previous research has suggested that different ginsenosides are capable of inducing cell cycle arrest at the G0/G1 phase. This arrest is achieved through the downregulation of cyclin D1 and CDK4 expression, as well as the

upregulation of p21 and p53 expression. When there is DNA damage, p53 either increases p21 levels or triggers apoptosis to stop the cell cycle.^[31,32] Our findings indicated that the expression of cyclin D1 and CDK4 protein levels decreased and the expression of p21 and p53 increased in CK-treated NSCLC cells and tumor tissues, indicating that CK induced G1 cell cycle arrest *in vivo* and *in vitro* in a dose-dependent manner.

Promoting apoptosis is a crucial approach to induce cell death in anticancer treatments. As a result, we noticed an increase in apoptosis of H460 and PC9 cells after CK treatment, as indicated by fluorescent staining and flow cytometry analysis in this work. Specifically, the results of Annexin V-FITC/PI double staining indicated a notable rise in the proportion of apoptotic H460 and PC9 cells. Moreover, the findings from Hoechst 33342 staining demonstrated that CK treatment led to a decrease in cell population and induced characteristic changes in the nuclei, including fragmentation, condensation, and the formation of apoptotic bodies. Furthermore, our findings confirmed that CK induced apoptosis and reduced MMP in NSCLC cells in a concentration-dependent manner. Apoptosis, a regulated form of cell death, is triggered by caspase enzymes belonging to the cysteine protease family. It is initiated through two principal pathways: the intrinsic pathway involving mitochondria and the extrinsic pathway involving death receptors.^[33] The mitochondrial apoptotic pathway is principally triggered by the Bcl-2 protein family, which also contains the anti-apoptotic protein Bcl-2 and the pro-apoptotic proteins Bax and Bad.^[34] Previous studies have shown that the anti-apoptotic protein Bax plays a role in activating caspase-9, initiating apoptosis. In contrast, the presence of Bcl-2 helps maintain cellular functionality and inhibits apoptosis through the mitochondrial pathway. The intrinsic pathway-induced apoptosis is facilitated by caspase-3, a protein that can activate downstream caspases and ultimately trigger apoptosis.^[35] Our findings indicated that CK-induced increased the expression of cleaved PARP, cleaved caspase-3, cleaved caspase-9, and Bax; decreased the level of Bcl-2, contributing to apoptotic cell death of NSCLC cells and tumor tissues. Therefore, these findings provide evidence that CK promotes apoptosis in non-small cell lung cancer cells via the intrinsic pathway.

Oxidative stress, caused by excessive oxidant generation and decreased antioxidant defense, can lead to inflammation, tumor progression, and drug resistance in cancer, while moderate levels can also benefit cancer processes.^[36] ROS plays dual roles in the context of the EGFR signaling pathway, acting both as mediators of the pathway and as regulators of the oxidation status and activation of the EGFR protein.^[37] In this study, we assessed the effect of CK on ROS production by staining cells with DCFH-DA. The results have shown that the intracellular level of ROS was significantly increased in a dose-dependent manner. Excessive production of ROS

results in cell cycle arrest and apoptosis, and ROS can serve as mediators of cellular signaling pathways, including the PI3K/Akt and MAPK pathways.^[38] Multiple studies have established a correlation between elevated EGFR expression in non-small cell lung cancer and unfavorable responses to chemotherapy, reduced survival rates, and frequent occurrence of lymph node metastases.^[39] The effects of ginsenoside Rg3 in inducing apoptosis by suppressing the expression of EGFR in human lung adenocarcinoma have been reported by researchers.^[40] The regulation of cancer cell proliferation, apoptosis, and metabolism is facilitated by EGFR via the mediation of downstream PI3K/AKT/mTOR and MAPK pathways.^[41] The PTEN/PI3K/AKT/mTOR pathway is a crucial intracellular signaling pathway that regulates cell cycle progression, cell proliferation, survival, and differentiation.^[42,43] The EGFR-PI3K-AKT-mTOR signaling pathway has become an effective target in cancer treatment.^[44,45] According to reports, CK inhibited osteosarcoma cell growth and survival, caused apoptosis, and prevented migration and invasion via the PI3K/mTOR/p70S6K1 signaling pathway.^[46] However, there was no study about the effect of ginsenoside CK on EGFR/PI3K/mTOR in NSCLC. In this study, we studied the effect of CK on the EGFR signaling pathway in NSCLC. The results have shown that CK significantly inhibited the phosphorylation of EGFR expression and its downstream proteins in NSCLC cells and tumor tissues. The PTEN/PI3K/Akt/mTOR pathway was also explored in this study, and it was found that CK suppressed p-PI3K, p-Akt, and p-mTOR but induced the expression of PTEN, leading to apoptotic cell death. Therefore, targeting the EGFR signaling pathway has profound effects on cell growth. Based on these experimental findings, it can be concluded that CK has the potential to suppress cell growth and induce cell death both *in vitro* and *in vivo*. Our findings suggested that CK could be a novel and valuable antitumor agent targeting NSCLC.

In conclusion, ginsenoside CK effectively inhibited cell proliferation by inducing G1 phase arrest and promoting apoptosis through the EGFR/PI3K/mTOR signaling pathway *in vitro* and *in vivo*. Additionally, CK inhibited the growth of H460 xenograft tumors in mice without creating any harm. These results strongly indicate that CK has the potential to serve as a novel and valuable therapeutic agent for targeting non-small cell lung cancer.

Author Contributions

Conceptualization, P.F., J.Z., and L.Q.; Methodology, P.F., J.Z., and L.Q.; Software, P.F., J.Z., and L.Q.; Validation, P.F., J.Z., and L.Q.; Formal analysis, P.F., J.Z., and L.Q.; Investigation, P.F., J.Z., L.Q., and D.F.; Resources, R.H., D.F., and X.M.; Data curation, P.F., J.Z., L.Q., and D.F.; Writing—original draft preparation, P.F., J.Z., and L.Q.; Writing—review and editing, P.F., J.Z., and L.Q.; Visualization, P.F., J.Z., and L.Q.; Supervision, D.F.;

Project administration, X.M., RH and D.F.; Funding acquisition, X.M., RH, and D.F.

Funding Information

This work was financially supported by the National Key R&D Program of China (2021YFC2101500), the National Natural Science Foundation of China (22078264 and 22108223), the Key R&D Program of Shaanxi (2022ZDLSF05-12), Natural Science Foundation of Shaanxi (2019JQ-259), Xian Association for Science and Technology Youth Talent Support Plan (095920211301), and the Xi'an Science and Technology Project (20191422315KYPT014JC016 and 20GXSF0004).

CONFLICT OF INTEREST

The authors declare that they have no known competing financial interests or personal relationships that could have appeared to influence the work reported in this paper.

Ethics Statement

Approval of the research protocol by an Institutional Reviewer Board.

Animal Studies: The experimental protocol involving animals received approval from the Animal Ethics Committee of Northwest University (NWU-AWC-20210304M).

Data availability statement

Data will be made available on request.

REFERENCES

1. A. Aggarwal, G. Lewison, S. Idir, M. Peters, C. Aldige, W. Boerckel, P. Boyle, E.L. Trimble, P. Roe, T. Sethi, The state of lung cancer research: a global analysis, *J. Thorac. Oncol*, 2016; 11: 1040–1050.
2. A. Rekowski, P. Rola, M. Wójcik-Superczyńska, I. Chmielewska, P. Krawczyk, J. Milanowski, Efficacy of Osimertinib in Lung Squamous Cell Carcinoma Patients with EGFR Gene Mutation—Case Report and A Literature Review, *Curr. Oncol*, 2022; 29: 3531–3539.
3. A.C. Borczuk, Updates in grading and invasion assessment in lung adenocarcinoma, *Mod. Pathol*, 2022; 35: 28–35.
4. R. Rajabalizadeh, M. Ghasemzadeh Rahbardar, H. Hosseinzadeh, Medicinal herbs in treating chemotherapy-induced nausea and vomiting: A review, *Phyther. Res.*, 2022.
5. H. Yuan, Q. Ma, L. Ye, G. Piao, The traditional medicine and modern medicine from natural products, *Molecules*, 2016; 21: 559.
6. Z.A. Ratan, M.F. Haidere, Y.H. Hong, S.H. Park, J.-O. Lee, J. Lee, J.Y. Cho, Pharmacological potential of ginseng and its major component ginsenosides, *J. Ginseng Res.*, 2021; 45: 199–210.
7. Y. Li, J. Lu, F. Bai, Y. Xiao, Y. Guo, Z. Dong, Ginsenoside Rg3 suppresses proliferation and induces apoptosis in human osteosarcoma, *Biomed*

- Res. Int., 2018; 2018.
8. Z. Duan, J. Deng, Y. Dong, C. Zhu, W. Li, D. Fan, Anticancer effects of ginsenoside Rk3 on non-small cell lung cancer cells: in vitro and in vivo, *Food Funct*, 2017; 8: 3723–3736.
 9. Y. Liu, D. Fan, The preparation of ginsenoside Rg5, its antitumor activity against breast cancer cells and its targeting of PI3K, *Nutrients*, 2020; 12: 246.
 10. S. Zhang, M. Zhang, J. Chen, J. Zhao, J. Su, X. Zhang, Ginsenoside compound K regulates HIF-1 α -mediated glycolysis through bclaf1 to inhibit the proliferation of human liver cancer cells, *Front. Pharmacol*, 2020; 11: 583334.
 11. S.J. Lee, J.S. Lee, E. Lee, T.-G. Lim, S. Byun, The ginsenoside metabolite compound K inhibits hormone-independent breast cancer through downregulation of cyclin D1, *J. Funct. Foods*, 2018; 46: 159–166.
 12. H. Shigematsu, A.F. Gazdar, Somatic mutations of epidermal growth factor receptor signaling pathway in lung cancers, *Int. J. Cancer*, 2006; 118: 257–262.
 13. K.S. Alharbi, M.A.J. Shaikh, O. Afzal, A.S.A. Altamimi, W.H. Almalki, S.I. Alzarea, I. Kazmi, F.A. Al-Abbasi, S.K. Singh, K. Dua, An overview of epithelial growth factor receptor (EGFR) inhibitors in cancer therapy, *Chem. Biol. Interact*, 2022; 110108.
 14. S. Sigismund, D. Avanzato, L. Lanzetti, Emerging functions of the EGFR in cancer, *Mol. Oncol*, 2018; 12: 3–20.
 15. J.W. Carlisle, S.S. Ramalingam, Role of osimertinib in the treatment of EGFR-mutation positive non-small-cell lung cancer, *Futur. Oncol*, 2019; 15: 805–816.
 16. M. Cabanero, M.S. Tsao, Circulating tumour DNA in EGFR-mutant non-small-cell lung cancer, *Curr. Oncol*, 2018; 25: 38–44.
 17. P. Minder, E. Zajac, J.P. Quigley, E.I. Deryugina, EGFR regulates the development and microarchitecture of intratumoral angiogenic vasculature capable of sustaining cancer cell intravasation, *Neoplasia*, 2015; 17: 634–649.
 18. H. Zhu, X. Cao, F. Ali-Osman, S. Keir, H.-W. Lo, EGFR and EGFRvIII interact with PUMA to inhibit mitochondrial translocation of PUMA and PUMA-mediated apoptosis independent of EGFR kinase activity, *Cancer Lett.*, 2010; 294: 101–110.
 19. S.-Y. Han, W. Zhao, H. Sun, N. Zhou, F. Zhou, G. An, P.-P. Li, *Marsdenia tenacissima* extract enhances gefitinib efficacy in non-small cell lung cancer xenografts, *Phytomedicine*, 2015; 22: 560–567.
 20. T. Shimoyama, F. Koizumi, H. Fukumoto, K. Kiura, M. Tanimoto, N. Saijo, K. Nishio, Effects of different combinations of gefitinib and irinotecan in lung cancer cell lines expressing wild or deletional EGFR, *Lung Cancer*, 2006; 53: 13–21.
 21. Y. Liang, T. Zhang, L. Ren, S. Jing, Z. Li, P. Zuo, T. Li, Y. Wang, J. Zhang, Z. Wei, Cucurbitacin Iib induces apoptosis and cell cycle arrest through regulating EGFR/MAPK pathway, *Environ. Toxicol. Pharmacol*, 2021; 81: 103542.
 22. Y. Peng, Y. Wang, C. Zhou, W. Mei, C. Zeng, PI3K/Akt/mTOR Pathway and Its Role in Cancer Therapeutics: Are We Making Headway?, *Front. Oncol*, 2022; 12: 819128.
 23. X. He, X. Liu, X. Chen, L. Bian, W. Zhao, J. Shen, Q. Sun, Gambogic acid induces EGFR degradation and Akt/mTORC1 inhibition through AMPK dependent-LRIG1 upregulation in cultured U87 glioma cells, *Biochem. Biophys. Res. Commun*, 2013; 435: 397–402.
 24. J.T. Hartmann, H.-P. Lipp, Toxicity of platinum compounds, *Expert Opin. Pharmacother*, 2003; 4: 889–901.
 25. R.S. Herbst, A.-M. Maddox, M.L. Rothenberg, E.J. Small, E.H. Rubin, J. Baselga, F. Rojo, W.K. Hong, H. Swaisland, S.D. Averbuch, Selective oral epidermal growth factor receptor tyrosine kinase inhibitor ZD1839 is generally well-tolerated and has activity in non-small-cell lung cancer and other solid tumors: Results of a phase I trial, *J. Clin. Oncol*, 2002; 20: 3815–3825.
 26. I. Solassol, F. Pinguet, X. Quantin, FDA-and EMA-approved tyrosine kinase inhibitors in advanced EGFR-mutated non-small cell lung cancer: safety, tolerability, plasma concentration monitoring, and management, *Biomolecules*, 2019; 9: 668.
 27. C.-H. Chiu, C.-M. Tsai, Y.-M. Chen, S.-C. Chiang, J.-L. Liou, R.-P. Perng, Gefitinib is active in patients with brain metastases from non-small cell lung cancer and response is related to skin toxicity, *Lung Cancer*, 2005; 47: 129–138.
 28. L. Chen, Y. Meng, Q. Sun, Z. Zhang, X. Guo, X. Sheng, G. Tai, H. Cheng, Y. Zhou, Ginsenoside compound K sensitizes human colon cancer cells to TRAIL-induced apoptosis via autophagy-dependent and-independent DR5 upregulation, *Cell Death Dis.*, 2016; 7: e2334–e2334.
 29. J.-M. Oh, E. Kim, S. Chun, Ginsenoside compound K induces ros-mediated apoptosis and autophagic inhibition in human neuroblastoma cells in vitro and in vivo, *Int. J. Mol. Sci.*, 2019; 20: 4279.
 30. H.K. Matthews, C. Bertoli, R.A.M. de Bruin, Cell cycle control in cancer, *Nat. Rev. Mol. Cell Biol.*, 2022; 23: 74–88.
 31. E.S. Helton, X. Chen, p53 modulation of the DNA damage response, *J. Cell. Biochem*, 2007; 100: 883–896.
 32. X. Deng, J. Zhao, L. Qu, Z. Duan, R. Fu, C. Zhu, D. Fan, Ginsenoside Rh4 suppresses aerobic glycolysis and the expression of PD-L1 via targeting AKT in esophageal cancer, *Biochem. Pharmacol*, 2020; 178: 114038.
 33. M. V. Fiandalo, N. Kyprianou, Caspase control: protagonists of cancer cell apoptosis, *Exp. Oncol*, 2012; 34: 165.
 34. B.G. Eimani, M.H. Sanati, M. Houshmand, M. Ataei, F. Akbarian, N. Shakhssalim, Expression and prognostic significance of bcl-2 and bax in the progression and clinical outcome of transitional

- bladder cell carcinoma, *Cell J.*, 2014; 15: 356. 43: 886–896.
35. M. Brentnall, L. Rodriguez-Menocal, R.L. De Guevara, E. Cepero, L.H. Boise, Caspase-9, caspase-3 and caspase-7 have distinct roles during intrinsic apoptosis, *BMC Cell Biol.*, 2013; 14: 1–9.
 36. D.T.N. Huynh, Y. Jin, C.-S. Myung, K.-S. Heo, Ginsenoside Rh1 induces MCF-7 cell apoptosis and autophagic cell death through ROS-mediated Akt signaling, *Cancers (Basel)*, 2021; 13: 1892.
 37. M.-S. Weng, J.-H. Chang, W.-Y. Hung, Y.-C. Yang, M.-H. Chien, The interplay of reactive oxygen species and the epidermal growth factor receptor in tumor progression and drug resistance, *J. Exp. Clin. Cancer Res.*, 2018; 37: 1–11.
 38. Y. Mi, C. Xiao, Q. Du, W. Wu, G. Qi, X. Liu, Momordin Ic couples apoptosis with autophagy in human hepatoblastoma cancer cells by reactive oxygen species (ROS)-mediated PI3K/Akt and MAPK signaling pathways, *Free Radic. Biol. Med.*, 2016; 90: 230–242.
 39. L. Belluomini, S.T. Riva, M. Simbolo, R. Nocini, I. Trestini, A. Avancini, D. Tregnago, M.G. Ferrara, A. Caldart, A. Dodi, Anticipating EGFR targeting in early stages of lung cancer: Leave no stone unturned, *Cells.*, 2021; 10: 2685.
 40. E.J. Joo, J. Chun, Y.W. Ha, H.J. Ko, M.-Y. Xu, Y.S. Kim, Novel roles of ginsenoside Rg3 in apoptosis through downregulation of epidermal growth factor receptor, *Chem. Biol. Interact.*, 2015; 233: 25–34.
 41. C. Stefani, D. Miricescu, I.-I. Stanescu-Spinu, R.I. Nica, M. Greabu, A.R. Totan, M. Jinga, Growth factors, PI3K/AKT/mTOR and MAPK signaling pathways in colorectal cancer pathogenesis: where are we now?, *Int. J. Mol. Sci.*, 2021; 22: 10260.
 42. H. Wang, J. Wang, J. Zhang, S. Jin, H. Li, Role of PI3K/AKT/mTOR signaling pathway in DBP-induced apoptosis of testicular sertoli cells in vitro, *Environ. Toxicol. Pharmacol.*, 2017; 53: 145–150.
 43. Y. Yang, S. Qiu, L. Qian, Y. Tian, Y. Chen, L. Bi, W. Chen, OCF can repress tumor metastasis by inhibiting epithelial–mesenchymal transition involved in PTEN/PI3K/AKT pathway in lung cancer cells, *PLoS One.*, 2017; 12: e0174021.
 44. W.W.B. de Kort, S. Spelier, L.A. Devriese, R.J.J. van Es, S.M. Willems, Predictive value of EGFR-PI3K-AKT-mTOR-pathway inhibitor biomarkers for head and neck squamous cell carcinoma: a systematic review, *Mol. Diagn. Ther.*, 2021; 25: 123–136.
 45. C. Treda, M. Popeda, M. Ksiazkiewicz, D.P. Grzela, M.P. Walczak, M. Banaszczyk, J. Peciak, E. Stoczynska-Fidelus, P. Rieske, EGFR activation leads to cell death independent of PI3K/AKT/mTOR in an AD293 cell line, *PLoS One*, 2016; 11: e0155230.
 46. K. Chen, J. Jiao, J. Xue, T. Chen, Y. Hou, Y. Jiang, L. Qian, Y. Wang, Z. Ma, Z. Liang, Ginsenoside CK induces apoptosis and suppresses proliferation and invasion of human osteosarcoma cells through the PI3K/mTOR/p70S6K1 pathway, *Oncol. Rep.*, 2020;